

## Supporting Information (SI)

### Methods

**Materials** Fmoc-*D*-Ala-OH, Fmoc-*L*-Lys(Boc)-OH, polystyrene-(2-chlorotrityl) resin (loading: 1.5 mmol/g), and 2-(1*H*-benzotriazole-1-yl)-1,1,3,3-tetramethyluronium hexafluorophosphate (HBTU) were purchased from Nova Biochem. 2-Propanephosphonic acid anhydride (T3P) in DMF was purchased from Advanced ChemTech. Polystyrene-*block*-poly(methyl methacrylate) (PS-*b*-PMMA) and carboxylic acid-terminated polystyrene (PS-COOH) ( $M_w=3K$ , *PDI* 1.4) were purchased from Polymer Source. Two PS-*b*-PMMA BCPs with molecular weight of 37K-37K (called “*LSM*”, *PDI* 1.07) and 57K-25K (called “*CSM*”, *PDI* 1.07), respectively, were used. Carboxylic acid-terminated poly(ethylene oxide) (PEO) ( $M_w=3.3K$ , *PDI* 1.2) was purchased from RAPP POLYMER. All reagents were purchased with the highest purity and used as received unless otherwise noted. The random copolymers of styrene and methyl methacrylate with 2% reactive benzocyclobutene (BCB) [P(S-*r*-BCB-*r*-MMA)] ( $M_w= 20.3K$  or  $14.7K$ , *PDI* 1.2) were provided by T. P. Russell at the University of Massachusetts, Amherst.

**Synthesis of cyclic peptide (8CP) and CP-polymer conjugates (PEO-8CP, PS-8CP and PMMA-8CP)** The linear precursor to the cyclic octapeptide [*D*-Ala-*L*-Lys]<sub>4</sub> (8CP) was prepared with standard Fmoc-based (Fmoc = 9-fluorenylmethoxycarbonyl) protocols for solid-phase peptide synthesis using a 2-chlorotrityl chloride resin preloaded with Fmoc-*L*-Lys(Boc)-OH. After cleavage of the linear octapeptide using 1% TFA in dichloromethane containing 5% triisopropyl silane, 8CP was cyclized head-to-tail using T3P and DIPEA. Boc-protecting groups were subsequently removed with a cleavage cocktail containing 95% TFA, 2.5% triisopropylsilane and 2.5% MilliQ water. Carboxylic acid-terminated PEO was conjugated to 8CP by coupling to the  $\epsilon$ -amino groups of lysine residues with a polymer to 8CP feed ratio of 8. PEO-8CP was purified by extensive dialysis (regenerated cellulose, MWCO 6-8 *kDa*) against MilliQ water. PS-8CP was prepared using a similar protocol. For PMMA-8CP, the amine group of the lysine residues was first modified with the STP-ester of 4-azidovaleric acid. Alkyne terminated PMMA was coupled to 8CP using standard copper-mediated “click” chemistry. The excess of PMMA was removed by subjecting the reaction mixture to standard reaction conditions in the presence of an azido-modified Merrifield resin.

**Thin film** Si substrates were modified using a random copolymer of styrene and methyl methacrylate as described previously<sup>[1]</sup>. A ~ 8-10 nm thin film of [P(S-*r*-BCB-*r*-MMA)] was spin coated onto the substrate and subsequently annealed at 250 °C for 15 minutes to crosslink random brush. The brush layer was rinsed with toluene 3 times at 3000 rpm to remove uncrosslinked polymers.

Polymer-8CP conjugates and PS-*b*-PMMA BCPs were dissolved in toluene and mixed overnight. Thin films were prepared by spin casting a 1 wt % solution in toluene at 3000 rpm. The films were annealed at 178 °C under vacuum for 4 h and slowly cooled down to room temperature over 15 minutes. For TEM measurements,

thin films were floated off the Si substrate by immersing in a 5wt % HF solution, rinsed in DI water bath, and transferred onto a copper grid. Membranes for proton and gas transport measurements were prepared similarly onto commercially available membrane (HT Tuffryn, Pall Life Sciences) with an average diameter of 0.2  $\mu\text{m}$  and thickness of 152  $\mu\text{m}$ .

**Grazing incidence small angle x-ray scattering (GISAXS)** measurements were performed at beamline 7.3.3 at the Advanced Light Source (ALS) at Lawrence Berkeley National Laboratory (LBNL) and at beamline 8-ID Advanced Photon Source (APS) at Argonne National Lab. An X-ray beam was directed at the sample at a grazing incident angle slightly above the critical angle of the polymer film. The scattered intensity was detected using a two-dimensional CCD camera with image sizes of 2304 x 2304 pixels.

**AFM** images were collected on the same samples used in the GISAXS experiments. Tapping mode SFM was used to study the thin film topography using a Molecular Imaging PicoSPM II with a PicoScan 2500 controller. Silicon cantilevers (RTESP from Veeco, Inc.) with a resonant frequency of 255 Hz were used.

**FTIR and ATR-FTIR** measurements were performed using a NICOLET 6700 FT-IR Spectrometer. For ATR-FTIR measurements, thin films with a thickness of  $\sim 100$  nm were used to achieve good signal-to-noise ratio. For in-situ FTIR, the samples were cast between two NaCl pellets. The heating/cooling rate is 20 degree per minute and each spectrum was collected 5 minutes after reaching targeted temperature.

**TEM** experiments were carried out at an accelerating voltage of 200 KeV using a JEOL 2100F STEM/TEM equipped with a Gatan Erlangshen ES500W, an Orius SC1000 CCDs, a Gatan Tridiem energy filter system, and a Gatan 806 high angle angular dark field (HAADF) STEM detector. For the STEM analysis, a 0.7 nm of probe size, 40  $\mu\text{m}$  of condenser aperture, and 7 cm of camera length of HAADF detector were used.

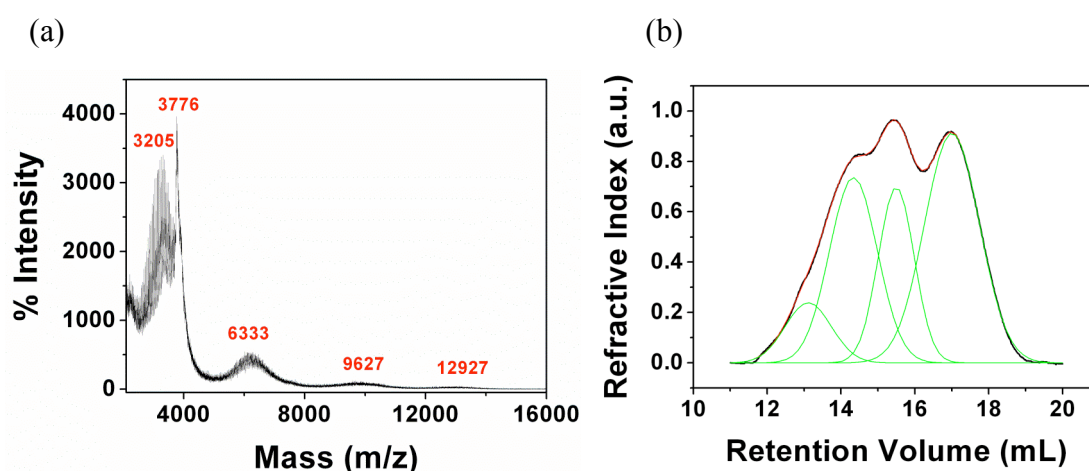
**Proton transport** measurements were carried out using a setup shown in Figure 4a. Briefly, 150  $\mu\text{L}$  of a 10  $\mu\text{M}$  solution of HPTS (8-Hydroxypyrene-1,3,6-trisulfonic acid trisodium salt) in 25 mM potassium phosphate buffer at pH 8.3 was added to a molded, transparent PDMS vessel. After covering the vessel with a prepared membrane, 50  $\mu\text{L}$  of 25 mM potassium phosphate buffer at pH 4.4 was introduced to the top of the membrane. Afterward, the UV-vis spectrum of the HPTS solution was recorded using a Hewlett-Packard 8453 spectrophotometer.

**Membrane permeability** measurements were carried out as described in detail in Figure S10.

## SI 1 Characterization of 8CP-polymer conjugates

Figure S1a shows the MALDI-TOF mass spectrum of PEO-8CP used in present study. Several groups of peaks associated with the conjugates were observed. We attribute the lowest molecular weight ( $M_w$ ) cluster with mean  $M_w$  of 3205 Da to residual unreacted PEO, while peaks around  $M_w$  3776 Da correspond to PEO-8CP conjugates with one PEG chain attached per CP. Similarly, the remaining three groups of peaks at 6333, 9627, 12927 Da correspond to PEO-8CP conjugates with 2, 3, 4 PEG chains attached to each CP, respectively. Figure S1b shows the size exclusion chromatogram of the dialyzed PEO-8CP using DMF containing 0.2% LiBr as eluent. The spectrum was decomposed into four Gaussian peaks, corresponding to PEO-8CP conjugates with different numbers of PEO chains attached per CP. Table S1 shows the estimated percentage of each conjugate in the mixture. From these estimates, the average number of PEO chains per CP is  $\sim 1.6$ . The peaks from free PEO and PEO-8CP with one PEO attached are too close to be distinguished. For the calculation, we assume the residual PEO is small and assume the elution peak corresponds to 1 arm conjugate. Thus, the real average number of PEO per 8CP may be slightly smaller.

**Figure S1**



(c) **Table S1** Areal percentage of PEO-8CPs with different number of PEO attached to each CP.

Molecular weight	Area (%)	Number of arms
3133	41.37	1
6263	20.57	2
9399	28.96	3
12969	9.10	4

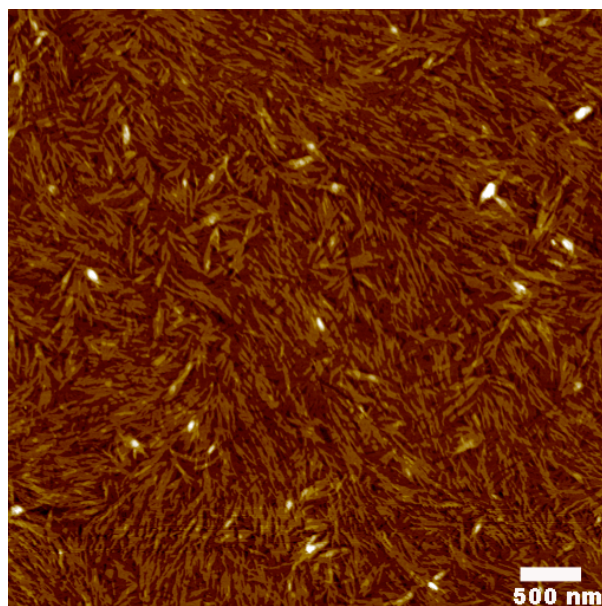
Similar analysis was carried out for 8CP-PS and 8CP-PMMA. However, we were unable to acquire MALDI-TOF spectra or GPC traces. The reason is unclear. Nevertheless PS-8CP was synthesized using the same chemistry and the molecular weight of PS is similar to that of PEO, we expect a similar number of PS chains conjugated to each CP. For PMMA-8CP, elemental analysis was performed and based on nitrogen content, the average number of conjugated PMMA chains per CP is estimated to be 3.3.

## SI 2 Characterization of CPNs and polymer-covered CPNs

Figure S2 (a) shows the SFM image of 8CPNs. The film was prepared by spin casting DMF solution of 8CP onto a silicon wafer, and dried under a stream of nitrogen. Aggregation of 8CPNs oriented parallel to the surface was observed. Figure S2 (b) shows the particle size distribution of 0.5mg/mL PEO-8CP in toluene obtained by Dynamic Light Scattering (DLS). PEO-8CPs form PEO-covered nanotubes, ~200 nm in length. Particle size distributions of 0.5mg/mL PMMA-8CP in toluene are shown in (c). The average length of PMMA-covered CPNs is shorter (~45nm) than that of PEO-8CPNs since PMMA molecular weight and the number of conjugated polymer chain per CP are higher. This is consistent with observations reported previously <sup>[2]</sup>. (d) shows the SFM image of PEO-8CPNs. The film was prepared by spin casting toluene solution of PEO-8CP onto a silicon wafer.

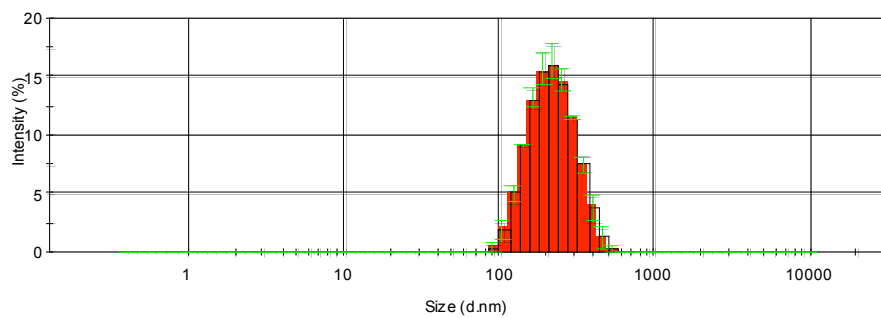
### Figure S2

(a)

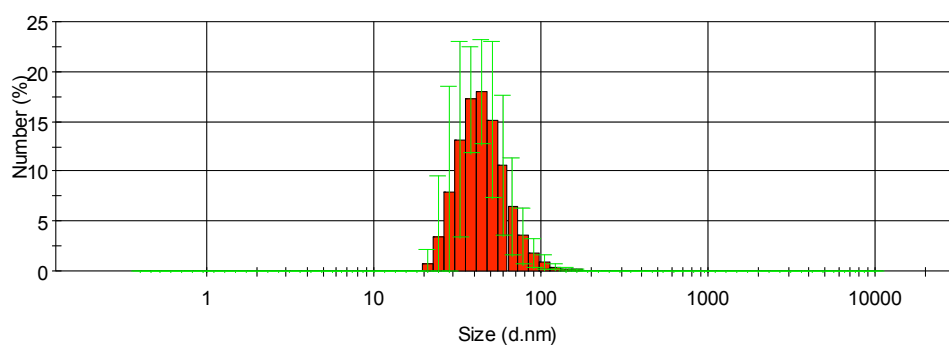


(b) PEO-8CP: Particle size distributions of 0.5M 8CP-PEO conjugate in toluene obtained by DLS.

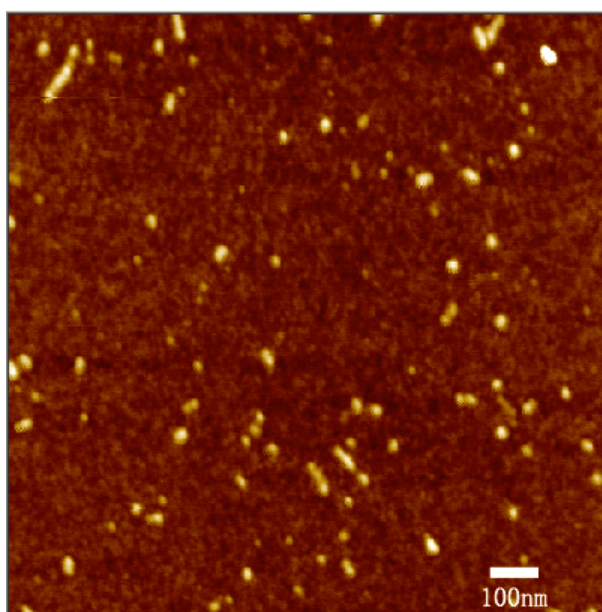
Diam. (nm)	% Intensity	FWHM (nm)
227	100	68.7
Diam. (nm)	% Volume	FWHM (nm)
249	100	81.2
Diam. (nm)	% Number	FWHM (nm)
227	100	100



(c) PMMA-8CP



(d) AFM image of PMMA-8CPN

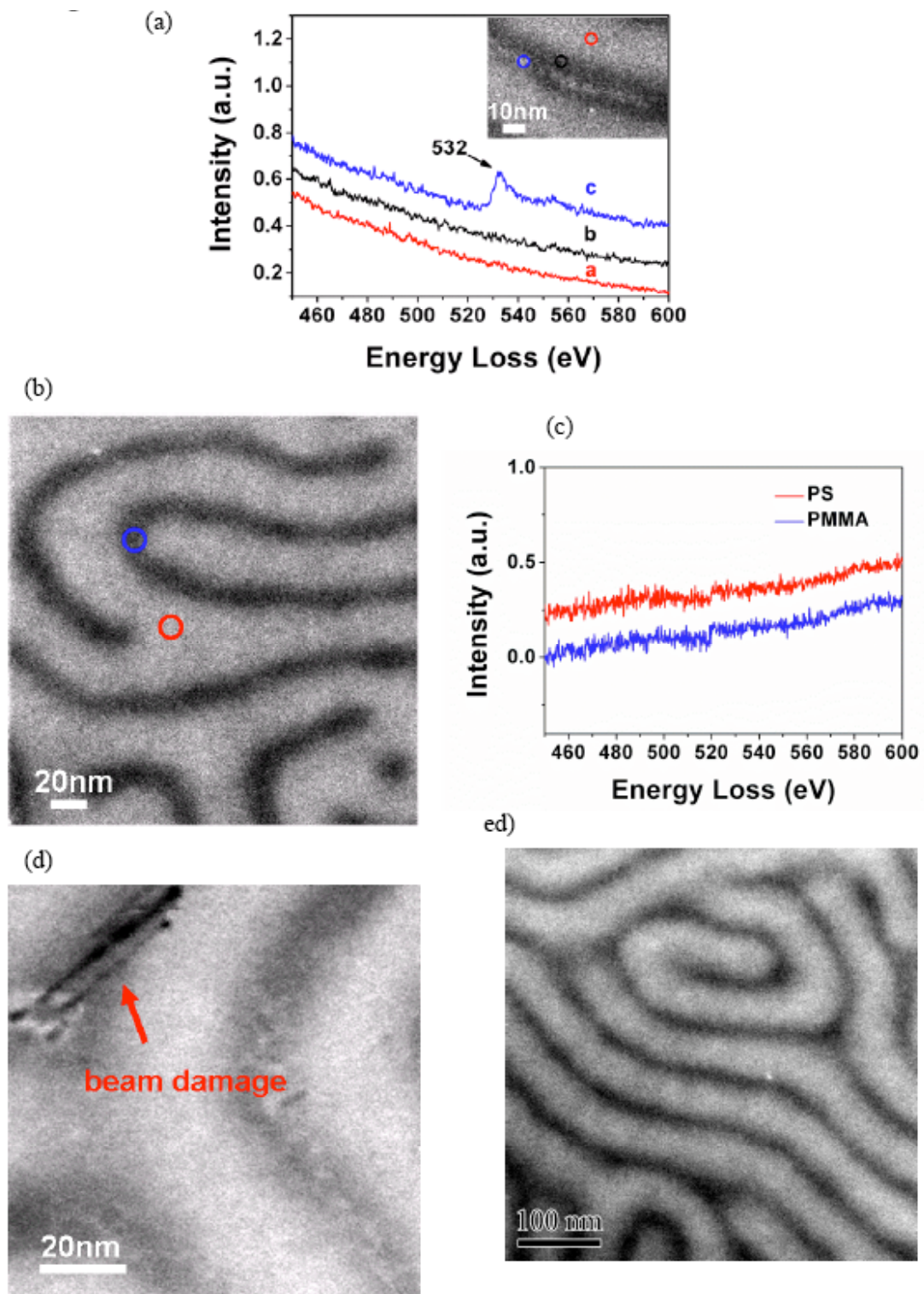


### SI 3

The contrast of a HAADF image is approximately proportional to  $Z^2$ , where  $Z$  is the average projected atomic numbers at the probe position. In the present experiments, the contrast between the different phases depends on the atomic numbers of elements comprising these phases and the density of each phase. The strain field in each phase or at the interface of different phases may also significantly influence the image contrast and their interpretations. For all HAADF-STEM images, PS phase appears brighter than PMMA. This is consistent with previous observations and may be contributed to the beam damage of PMMA. In Figure 3c, short bright strips or close packing dots at the center of PMMA lamellae are also observed. Under careful scrutiny, we can find that dark contrast features exist inside PEO-CPN with an approximate width of  $<1$  nm that corresponds to the diameter of 8CPN.

Figure S3 (a) The EELS spectra collected from a  $\sim 32$  nm thin film of PEO-8CP/LSM at three regions indicated by black, blue and red circles, respectively that identify PEO, PS and PMMA. Corresponding HAADF-STEM image is shown in Figure 3c. (b) shows the HAADF-STEM image of a  $\sim 32$  nm thin film of LSM acquired with the probe size of 0.7 nm. No features corresponding to CPNs were seen. (c) shows the EELS spectra collected from PMMA and PS lamellae indicated by blue and red circles, respectively. The beam damage for PMMA under the irradiation of high energy and high density electron beam is severe and absorption spectrum of oxygen near K-edge could not be observed. Beam damage can be clearly seen in the HAADF-STEM image of LSM thin film shown in (d) after attempts to acquire the EELS spectra of PMMA lamellae. (e) shows the HAADF-STEM image of a  $\sim 32$  nm thin film of PEO/LSM acquired with the probe size of 0.7 nm. For PEO/LSM thin films, we were not able to identify the spatial distribution of PEOs. We noticed that under electron beam, the stability of PEO-8CP/LSM thin films is higher than that of LSM or PEO/LSM.

Figure S3



SI 4

Figure S4

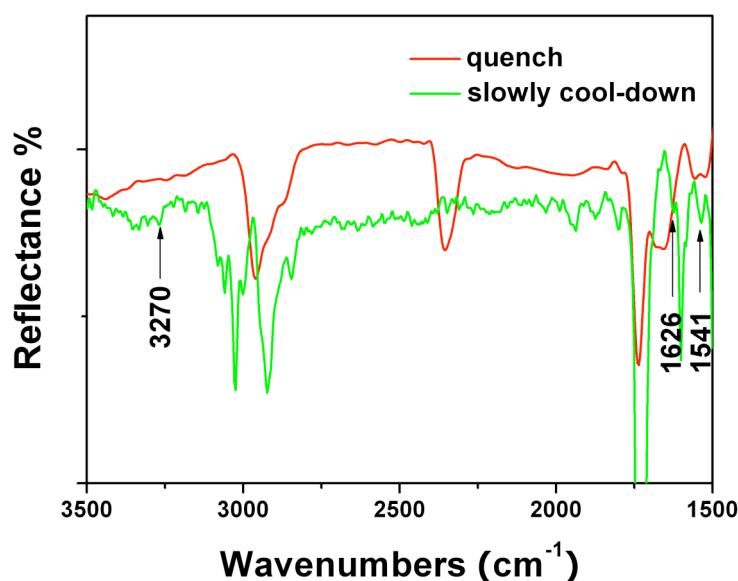


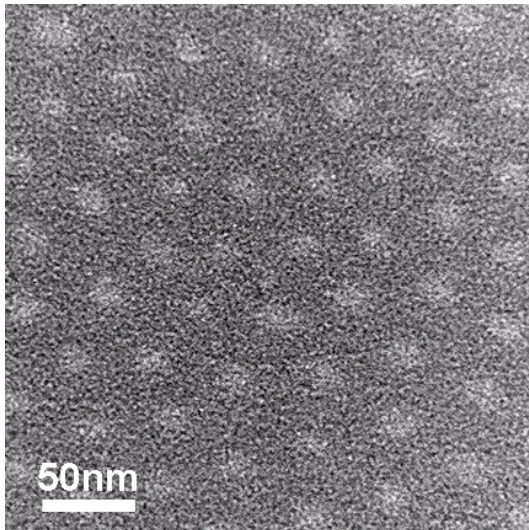
Figure S4 shows the FTIR spectra of thin films a PEO-8CP/CSM blend (2:10 *wt* ratio) that have been quenched and slowly cooled-down from 178°C to room temperature, respectively. To obtain reasonable signal-to-noise ratio, films with thickness of ~100 nm were used. The thin film that was slowly cool-down shows distinctive absorption peaks at 1626 and 1541  $\text{cm}^{-1}$  (corresponding to carbonyl “amide I & II” stretches), and ~ 3270  $\text{cm}^{-1}$  (corresponding to amine “amide A” stretch), confirming the existence of an extended H bonded,  $\beta$ -sheet-type structure, and the formation of PEO-8CPNs. However these diagnostic peaks of  $\beta$ -sheet-type structure were not seen in the quenched sample. Upon annealing at elevated temperature, a large fraction of hydrogen bonds between the amino acid residues on adjacent rings were broken. PEO-8CPs were selectively sequestered within PMMA microdomains. Upon cooling, PEO-8CPs re-assemble and form PEO-covered nanotubes in a PMMA cylindrical microdomains, leading to the hierarchically structured sub-nanometer porous films shown in Figure 4a.

## SI 5

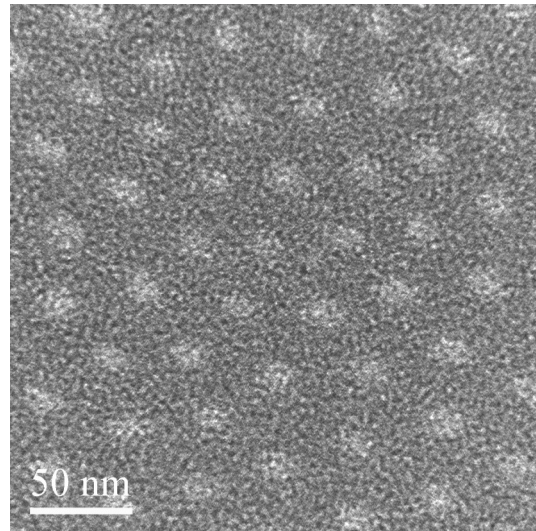
Figure S5 shows TEM bright field image of a ~32 nm thin film of (a) CSM and (b) PEO/CSM blend taken under the same condition as Figure 4b. There are no obvious bright spots indicating hollow nanotubes in the center of PMMA microdomains.

**Figure S5**

(a)



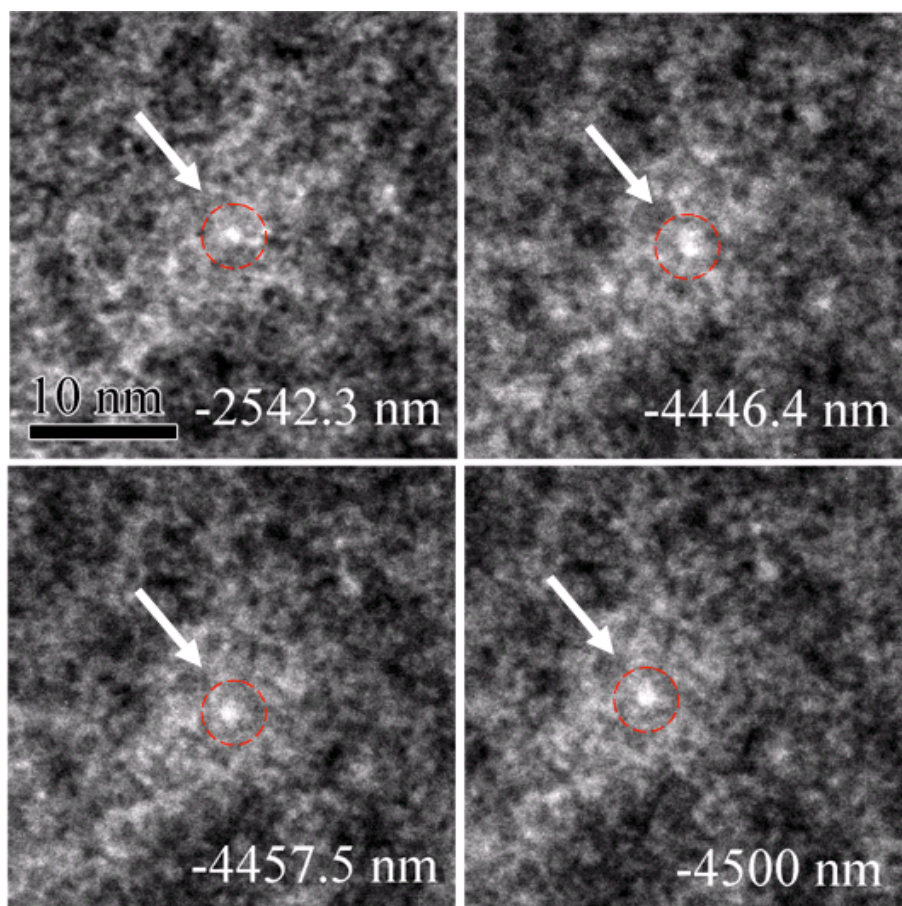
(b)



## SI 6

Figure S6 shows a series of energy filtered under-focus bright field TEM image of a  $\sim 32$  nm thin film of PEO-8CP/CSM blend. The under-focus distance at which the image was collected is noted in each image. The white dot indicated by an arrow corresponds to the top-view of 8CPN. When the phase contrast was varied, the CPNs can still be seen, however, speckles disappear.

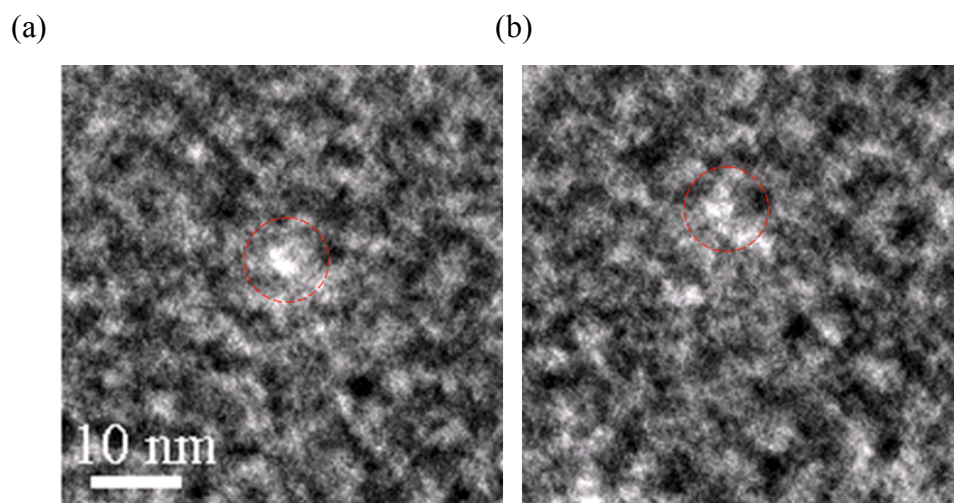
**Figure S6**



## SI 7

Figure S7 shows the TEM images of a  $\sim 32$  nm thin film of PEO-8CP/CSM blend before (a) and after (b) tilting two degrees along x- and y-axes. Due to the high aspect ratio of CPN ( $>40$ ), a slight tilt prevents direct top-view of the CPNs and only CPNs oriented perpendicular to the surface of the film can be seen.

**Figure S7**

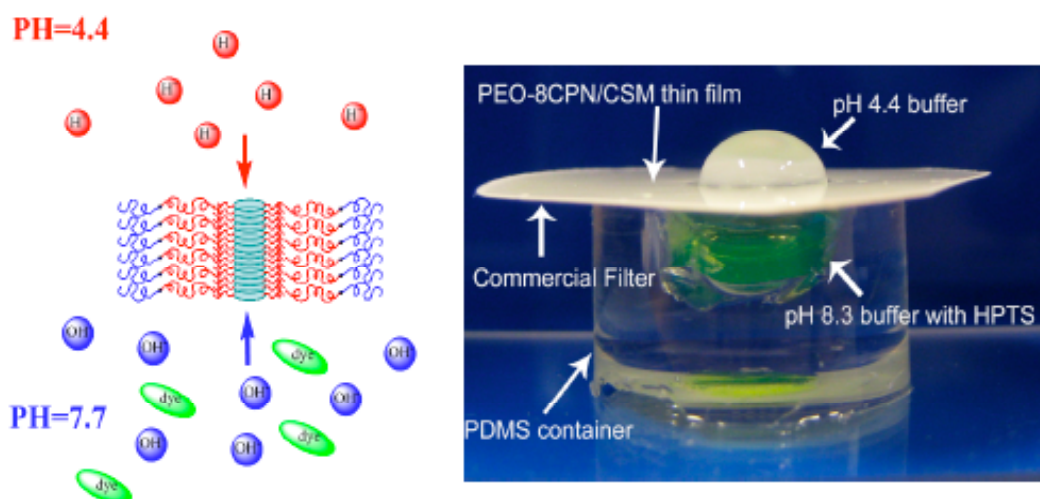


## SI 8

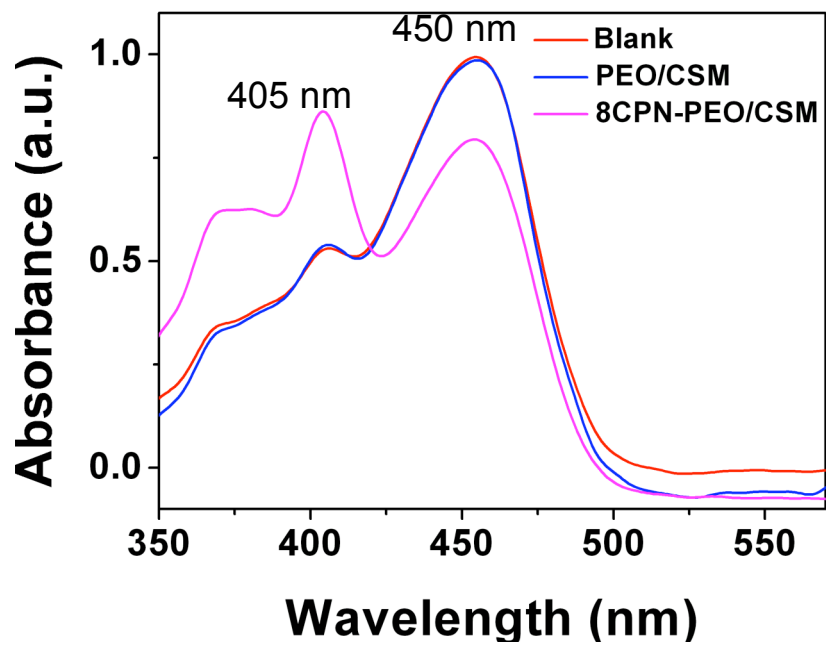
Transport studies of PEO-8CPN/CSM thin films. (a) shows the experimental setup for proton transport measurement. Test thin films were first prepared on silicon substrates with a 200 nm thermally grown silicon oxide layer and delaminated from the substrate by dipping into 5% aqueous HF before being transferred to the top of commercial membranes (HT Tuffryn, Pall Life Science). The indicator solution (10  $\mu$ M HPTS in 25mM  $K_2HPO_4$  with 10mM KCl at pH 8.3) was deposited into a 150  $\mu$ L PDMS container and covered with one of the fabricated thin film membranes. Subsequently, 50  $\mu$ L of 25mM  $K_2HPO_4$  at pH 4.4 was introduced to the top of the thin film. The UV-vis spectrum of HPTS buffer solution was collected after 2 minutes. (b) shows the UV-vis absorption spectra of HPTS buffer solution before and after the acidic buffer solution was deposited onto the PEO-8CPN/CSM and PEO/CSM thin films. For PEO/CSM thin films, no pH change was observed. In contrast, the decrease in pH for the HPTS buffer solution was clearly seen for PEO-8CPN/CSM thin films due to the proton transport through the CP nanotubes, which is consistent with PEO-8CPNs spanning the entire film thickness. (c) shows the peak intensity ratio between 450 nm and 405 nm, an indication of pH value of the buffer solution, at different time for PEO-8CPN/CSM, PEO/CSM and CSM membranes, confirming proton transport through the 8CPNs.

**Figure S8**

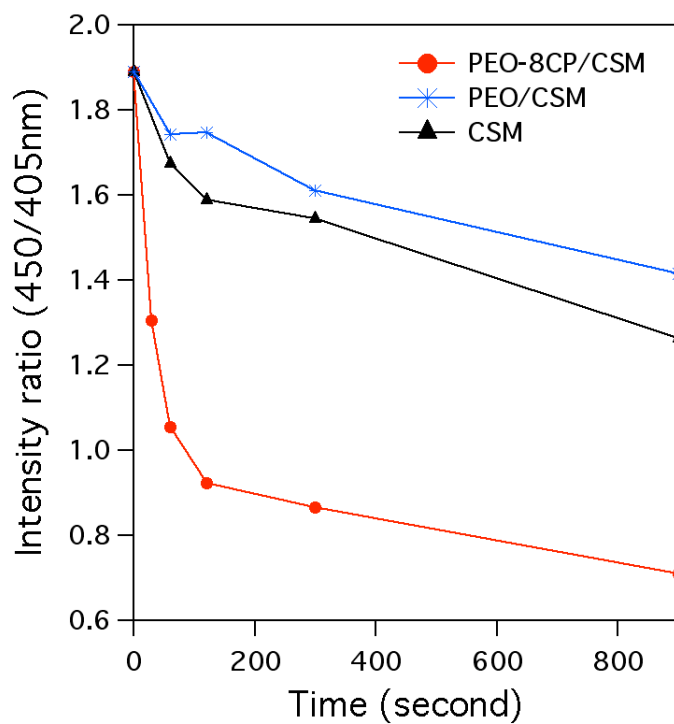
(a)



(b)



(c)



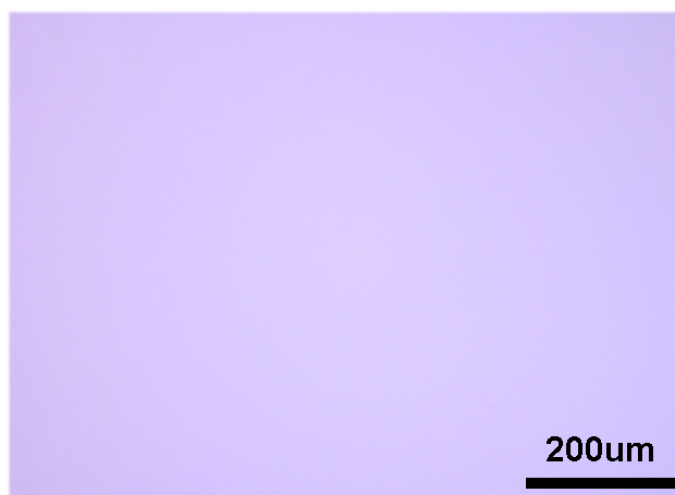
## SI 9

To ensure the membrane integrity for the proton transport measurement, the permeance of the PEO-8CPN/CSM membrane was measured using setup shown in Figure S10. After the proton transport measurement, the permeance of PEO-8CPN/CSM membrane was measured. It confirmed the integrity of the membrane and there is no leakage in the membrane. Figure S9 shows optical images of a representative membrane tested at different magnifications.

**Figure S9**



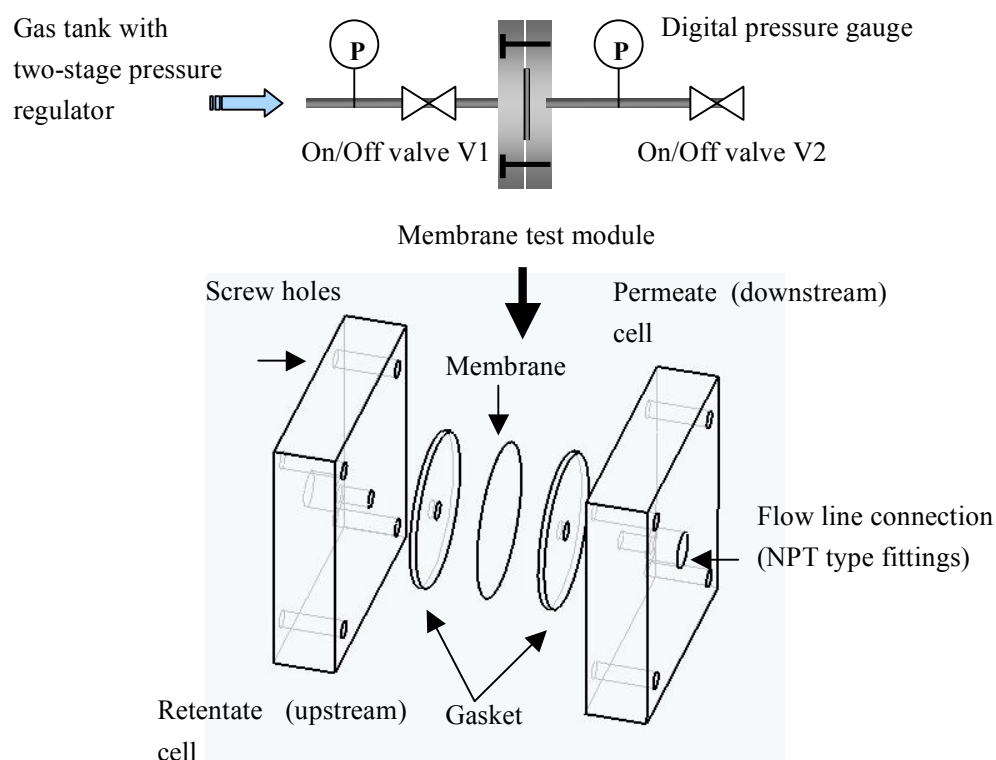
Zoom-in view of the center of the test membrane



## SI 10

Figure S10 shows the experimental setup for membrane permeability measurements. The membrane was sandwiched between two Viton<sup>®</sup> gaskets with a 1/8" hole at the center. The module was screw tightened. Measurements were carried out in the following procedure: First, valve V1 was closed and valve V2 was opened. After the upstream gas pressure was regulated to the specified pressure (in this case 1.5 psig), V1 was opened. V2 was then closed and the timer was started. The permeate cell pressure began to rise from 0 psig with time.

**Figure S10**



Permeance ( $\Pi$ ) of a membrane is defined as:

$$J = \Pi (P_{retentate} - P_{permeate}) \quad (\text{S10-1})$$

where  $J$  is the molar flux ( $\text{kmol/m}^2$ ) of the gas through the membrane,  $P_{retentate}$  and  $P_{permeance}$  are pressures of the retentate (upstream) cell and the permeance (downstream) cell, respectively.

Based on mass balance, the expression for permeance of the membrane can be derived [4].

$$\Pi = \frac{V}{A \cdot R_u \cdot T \cdot t} \ln \left[ \frac{P_{retentate}}{P_{retentate} - P_{permeance}(t)} \right] \quad (\text{S10-2})$$

where  $V$  is the volume of the permeate cell,  $A$  is the membrane area exposed to the gas stream,  $R_u$  is the universal gas constant,  $T$  is the temperature,  $P_{permeance}(t)$  is the pressure of permeance cell at an instance time ( $t$ ) during the measurement. All parameters are in SI units. Pressures here are gauge pressures in the unit of Pascal. Utilizing equation (S11-2) and the experimental data of  $P_{permeance}(t)$ , the permeance of each membrane ( $\Pi$ ) were obtained and listed in Table S2. Measurements were also performed using a commercial filter (the substrate of the membrane) and the result was consistent with the factory specified value. Note that values listed in Table S2 are the “overall permeance” for each membrane including the polymer film and the substrate filter. The “overall permeance” of the membrane is different from the permeance of the sub-nanometer pores ( $\Pi_{CPN}$ ) listed in Table S3, as will be discussed in SI 11.

**Table S2**

membrane <i>gas type</i>	“overall permeance” ( $\Pi$ ) [mol/m <sup>2</sup> sPa]	Number of samples
PEO/CSM <i>CO<sub>2</sub></i>	$3.46 \cdot 10^{-6} \pm 6.54 \cdot 10^{-7}$	11
PEO-8CPN/CSM <i>CO<sub>2</sub></i>	$7.86 \cdot 10^{-6} \pm 8.97 \cdot 10^{-7}$	11
PEO-8CPN/CSM <i>Neopentane</i>	$6.00 \cdot 10^{-6} \pm 4.21 \cdot 10^{-7}$	8

## SI 11

Gas permeance of sub-nanometer CPN pores is on the order of  $10^{-6}$  mol/m<sup>2</sup>sPa, which is over four orders of magnitude greater than what predicted from the classical gas flow theory. This indicates that gas transport through sub-nanometer CPN is ballistic in nature, which can be described by the Knudsen diffusion theory.

From free molecule flow theory, the Knudsen diffusion gas molar flux through a single pore is <sup>[5]</sup>:

$$J_{pore,Knudsen} = \frac{2}{3} \left( \frac{8}{\pi M R_u T} \right)^{1/2} \left( \frac{r_p}{L_f} \right) (\Delta P) \quad , \quad (S11-1)$$

where  $M$  is gas molecular weight,  $R_u$  is the universal gas constant.  $T$  is the temperature (assumed 300 K),  $r_p$  is pore radius,  $L_f$  is length of the pore, and  $\Delta P$  is the pressure difference across the pore.

From definition, the permeance of a single CPN pore based on Knudsen diffusion model is given by:

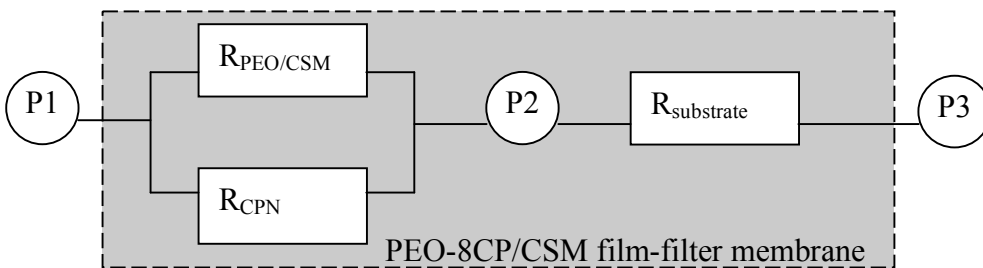
$$\Pi_{pore,Knudsen} = \frac{2}{3} \left( \frac{8}{\pi M R_u T} \right)^{1/2} \left( \frac{r_p}{L_f} \right) \quad (S11-2)$$

The permeance of CPN pores per unit membrane area calculated by Knudsen diffusion model is thus:

$$\Pi_{CPN,Knudsen} = a_{pore} \Pi_{pore,Knudsen} = \frac{2}{3} \left( \frac{8\pi}{M R_u T} \right)^{1/2} \left( \frac{N_p r_p^3}{L_f} \right) \quad , \quad (S11-3)$$

where  $a_{pores}$  = area fraction of CPN pores =  $N_p (\pi r_p^2)$ , and  $N_p$  is the number of pores/unit membrane area.

**Figure S11**



Gas flow through the PEO-8CP/CSM membrane can be evaluated analogous to the current of an equivalent circuit as shown in Figure S13, where.

$$J_{PEO-8CP/CSM} = \frac{(P_1 - P_3)}{(R_{CPN}^{-1} + R_{PEO/CSM}^{-1})^{-1} + R_{substrate}} = \Pi_{PEO-8CP/CSM} (P_1 - P_3) \quad , \quad (S11-4)$$

$$R_{PEO/CSM} = \frac{1}{(1 - a_{pores}) \Pi_{PEO/CSM}} \quad , \quad R_{CPN} = \frac{1}{\Pi_{CPN}} \quad , \quad \text{and} \quad R_{substrate} = \frac{1}{\Pi_{substrate}} \quad .$$

The permeance of CPN pores per unit membrane area from measurements ( $\Pi_{CPN}$ ) can thus be obtained by using Equation (S11-4) and experimental data (mean values) of  $\Pi_{PEO/CSM}$  ,  $\Pi_{PEO-8CP/CSM}$  and  $\Pi_{substrate}$  .

Table S3. Enhancement of gas flow rate through PEO-8CPN/CSM membranes in comparison to the theoretical values calculated using Knudsen diffusion model

Gas type	$\Pi_{CPN,experiment}$ [mol/m <sup>2</sup> sPa]	$\Pi_{CPN,Knudsen}$ [mol/m <sup>2</sup> sPa] (Equation S14-3)	Enhancement over Knudsen diffusion
CO <sub>2</sub>	5.69*10 <sup>-6</sup>	1.17*10 <sup>-7</sup>	<b>48.63</b>
Neopentane	3.26*10 <sup>-6</sup>	9.11*10 <sup>-8</sup>	<b>35.78</b>

### References:

1. Ryu, D. Y., Shin, K., Drockenmuller, E., Hawker, C. J. & Russell, T. P. A generalized approach to the modification of solid surfaces. *Science*, **308**, 236 (2005)
2. Couet, J.& Biesalski, M. Conjugating self-assembling rigid rings to flexible polymer coils for the design of organic nanotubes, *Small* **4**, 1008 (2008).
3. Hartgerink, J. D., Granja, J. R., Milligan, R. A. & Ghadiri, M. R. Self-assembling peptide nanotubes. *Journal of the American Chemical Society*, **118**, 43 (1996).
4. Acharya, M., Raich, B. A. & Foley, H. C. Metal-Suported Carbogenic Molecular Sieve Membranes: Synthesis and Applications, *Ind. Eng. Chem. Res.* **36**, 2924 (1997).
5. Mills, A. F. Mass Transfer, *Prentice-Hall Inc.* New Jersey, (2001)